

# BrainCognizer: Brain Decoding with Human Visual Cognition Simulation for fMRI-to-Image Reconstruction

Guoying Sun<sup>1</sup> Weiyu Guo<sup>2</sup> Tong Shao<sup>1</sup> Yang Yang<sup>1</sup> Haijin Zeng<sup>3</sup> Jie Liu<sup>1</sup> Jingyong Su<sup>1\*</sup>

1. School of Computer Science and Technology, Harbin Institute of Technology (Shenzhen), China

2. Thrust of Artificial Intelligence, The Hong Kong University of Science and Technology (Guangzhou), China

3. Department of Psychiatry, Harvard University, USA

**Abstract**—Brain decoding is a key neuroscience field that reconstructs the visual stimuli from brain activity with fMRI, which helps illuminate how the brain represents the world. fMRI-to-image reconstruction has achieved impressive progress by leveraging diffusion models. However, brain signals infused with prior knowledge and associations exhibit a significant information asymmetry when compared to raw visual features, still posing challenges for decoding fMRI representations under the supervision of images. Consequently, the reconstructed images often lack fine-grained visual fidelity, such as missing attributes and distorted spatial relationships. To tackle this challenge, we propose BrainCognizer, a novel brain decoding model inspired by human visual cognition, which explores multi-level semantics and correlations without fine-tuning of generative models. Specifically, BrainCognizer introduces two modules: the Cognitive Integration Module which incorporates prior human knowledge to extract hierarchical region semantics; and the Cognitive Correlation Module which captures contextual semantic relationships across regions. Incorporating these two modules enhances intra-region semantic consistency and maintains inter-region contextual associations, thereby facilitating fine-grained brain decoding. Moreover, we quantitatively interpret our components from a neuroscience perspective and analyze the associations between different visual patterns and brain functions. Extensive quantitative and qualitative experiments demonstrate that BrainCognizer outperforms state-of-the-art approaches on multiple evaluation metrics. Our code is released publicly at <https://github.com/Grace160/BrainCognizer>.

**Index Terms**—Brain decoding, fMRI-to-Image reconstruction, Latent diffusion model, Human visual cognition.

## I. INTRODUCTION

A challenging goal in neuroscience is to decode information from brain activity. The functional magnetic resonance imaging (fMRI) signals with changes in brain oxygen levels reflect the brain activity in response to external stimuli [1]. fMRI-to-image reconstruction [2]–[4] aims to reconstruct visual stimuli from fMRI signals, bridging brain activity and perception. Due to the scarcity of fMRI-image pairs [5], [6] and the inherently low signal-to-noise ratio [7] of fMRI caused by

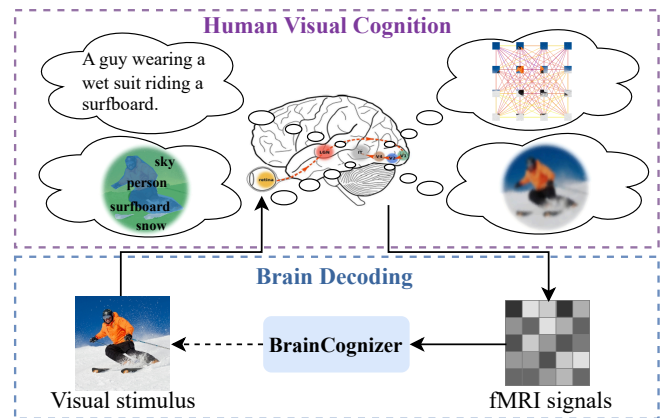


Fig. 1. The brain decoding process by simulating the human visual cognition. BrainCognizer extracts (1) coarse-grained semantics from captions, (2) fine-grained visual prior knowledge, (3) regional contextual relationships, and (4) low-level visual features for fMRI decoding and reconstruction.

attentional distractions and associative interferences during data collection, traditional voxel-to-pixel methods [8]–[11] often generate blurry images with poor semantic consistency.

Recently, the emergence of cross-modal foundation models such as CLIP [12], alongside the rapid advances in generative techniques like diffusion models [13]–[15], has led to substantial breakthroughs in fMRI-to-image reconstruction. The current pipeline of fMRI-to-image reconstruction [16]–[19] employs an encoder to learn neural representations from fMRI signals, which are aligned with features extracted by images. Features reflecting visual information decoded from brain activity serve as semantic conditions for diffusion models, which leverages rich priors and strong generative capabilities to produce high-fidelity image reconstructions. Therefore, the fMRI-to-image task is simplified to aligning fMRI-derived features with image representations obtained from foundation models, enabling the exploration of their encoding capabilities.

However, fMRI representation decoding under the direct supervision of CLIP features is often prone to overfitting [20], which we believe is essentially caused by dimension discrep-

\* Corresponding author, email-to: [sujingyong@hit.edu.cn](mailto:sujingyong@hit.edu.cn)

ancy. fMRI signals encode complex and diverse neural representations, encompassing both low-level visual perceptions (such as color, shape [21], and layout [22], [23]) and high-level cognitive features (including semantic categories, memory associations, and subjective experiences [24]). In contrast to *low-dimensional* CLIP features which are manually designed and primarily capture visual categories, fMRI signals serve as extremely *high-dimensional* carriers of rich brain information.

Consequently, this significant discrepancy in dimensionality leads to an *information asymmetry*, hindering effective semantic decoding from complex fMRI signals to guide diffusion. Existing methods [17], [19], [25] fail to address the representational gap and ignore the inherent information asymmetry, thereby impeding the reconstruction of fine-grained details, including semantic attributes, spatial relationships, and contextual information, which are shown in Fig. 2.

To tackle the challenge, we propose a novel brain decoding model, **BrainCognizer**, which enhances the hierarchical semantics and maintains region contextual correlations through the simulation of human visual cognition. As illustrated in Fig. 1, BrainCognizer enhances the fMRI decoding by leveraging prior knowledge derived from human visual cognition, effectively mitigating the reconstruction quality degradation caused by information asymmetry.

Specifically, we first propose the *Cognitive Integration Module (CIM)* to enhance the diversity of hierarchical region semantics by simulating the human visual holistic perception [26]. Subsequently, we propose the *Cognitive Correlation Module (CCM)*, which captures inter-region semantic differences and contextual relationships by topological correlation, simulating the brain differential perception [27], [28]. BrainCognizer leverages prior knowledge from human cognition to skillfully uncover semantics that guide the diffusion effectively, without any fine-tuning of the generative model.

Furthermore, we perform neuroscientific analyses of the embedded semantic and relational representations, thereby enhancing functional interpretability from a cognitive perspective. In summary, our contributions are as follows:

- 1) We propose BrainCognizer, a fine-grained brain decoding framework that mitigates information asymmetry by exploring hierarchical semantics and region contextual relations without fine-tuning of generative models.
- 2) We propose CIM and CCM inspired by human visual cognition, and quantitatively interpret them via brain function visualization, revealing that our method explores more fMRI voxels for decoding.
- 3) Extensive experimental results demonstrate the qualitative and quantitative fidelity of BrainCognizer, which achieves state-of-the-art performance on multiple evaluation metrics.

## II. RELATED WORK

### A. Visual Stimulus Decoding from fMRI.

Previous methods [6], [11], [16], [18], [29]–[32] decode fMRI features directly supervised by CLIP features, and use them to guide the diffusion. However, the large modality gap



Fig. 2. Image reconstruction examples. The highlighted regions indicate comparison. Existing methods fail to reconstruct fine-grained semantic attributes, such as the snow in the 1st row or the umbrella and sunglasses in the 3rd row. They also fail to recover contextual layouts, such as the people in the 2nd row. Our BrainCognizer effectively mitigates these issues.

between fMRI and CLIP features, combined with the limited amount of annotated data, leads to overfitting.

Methods [5], [6] attempt to alleviate it by leveraging large-scale unimodal or unlabeled data through self-supervised learning. MindBridge [19] narrows the modality gap by leveraging multi-subject data to enhance individual generalization. Nevertheless, their effectiveness is hindered by inter-subject variability. MindDiffuser [25] further enhances image fidelity via post-processing with semantic constraints. In addition, MindEye [17] improves the encoder architecture to enhance the representational capacity of fMRI decoding.

These methods overlook the fact that the fundamental cause of the modality gap lies in the information asymmetry between fMRI signals with rich prior knowledge and CLIP visual features. To address this issue, we propose BrainCognizer, which enhances the fMRI decoding by leveraging prior knowledge from human visual cognition, mitigating the reconstruction quality degradation caused by information asymmetry.

### B. Foundation Models for Visual Decoding.

Generation models have been widely applied in visual reconstruction. GAN-based methods [8], [10], [11], [30], [33] generate blurry images that lack semantic content, whereas recent studies [16]–[19] show that diffusion significantly improves both image quality and semantic fidelity.

fMRI signals are decoded under the supervision of CLIP features, and then used to guide the diffusion generation. CLIP [12] provides an effective representation space with structural similarities to the human brain [34], [35] and exhibits superior explanatory power for cortical activity [36], significantly facilitating fMRI decoding. To leverage more comprehensive CLIP semantics, Versatile Diffusion model [15]

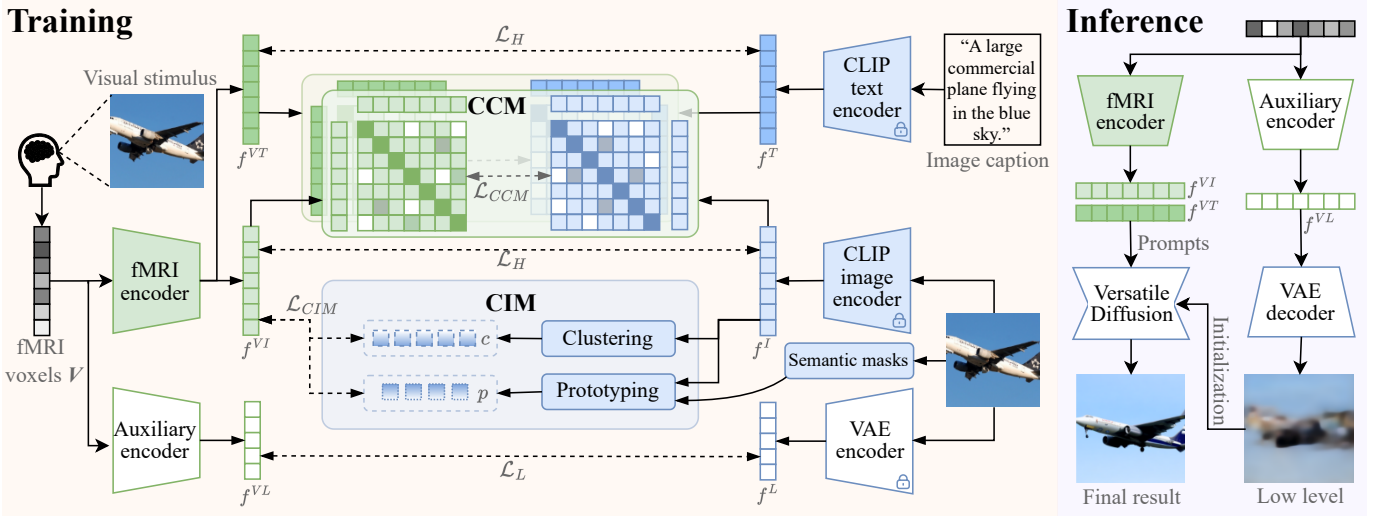


Fig. 3. The framework of BrainCognizer. CIM and CCM simulate human visual cognition to extract intrinsic information, guiding fMRI for more comprehensive representations. During inference, the outputs of the auxiliary encoder initialize the diffusion process and subsequently the fMRI features serve as prompts to constrain the reconstruction of the visual stimulus.

conditions the generation process on both text and image features of CLIP, thereby improving image fidelity.

Furthermore, the VAE [37] in the diffusion captures low-level visual codebooks. By mapping fMRI signals into the VAE latent space, the reconstruction process starts from a semantically blur prior instead of random noise, thus mitigating the stochasticity introduced by diffusion and improving reconstruction fidelity.

### III. METHOD

Inspired by the human visual cognition, we propose a novel fMRI-to-image reconstruction method, BrainCognizer, to improve the inadequate characterization caused by the information asymmetry between fMRI and images. BrainCognizer mainly comprises the Cognitive Integration Module (CIM) for intra-region semantic feature aggregation and the Cognitive Correlation Module (CCM) for inter-region topological correlations. The overview of BrainCognizer is illustrated in Fig. 3.

#### A. Pipeline

To decode richer visual patterns from fMRI, we propose a novel pipeline for fMRI-to-image reconstruction. It extracts low-level visual details through the VAE and decodes multi-level semantic representations via CLIP, while utilizing the Versatile Diffusion (VD) [15] to reconstruct visual images. VD takes the low-level results as the initial latent of VAE and generates the final reconstruction guided by the conditions of multi-level semantic representations.

For decoding low-level visual attributes, such as spatial structure and color composition, we introduce a lightweight auxiliary encoder composed of CNN and MLP. It decodes low-level features  $\mathbf{f}^{VL} \in \mathbb{R}^{4 \times 64 \times 64}$  from fMRI and aligns them with the latents  $f_L$  of VAE by mean absolute error loss, enabling the low-level blur perception from brain activity:

$$\mathcal{L}_L = |\mathbf{f}^L - \mathbf{f}^{VL}|. \quad (1)$$

For the decoding of high-level semantic information, we incorporate a dual-head fMRI encoder to extract features  $\mathbf{f}^{VI} \in \mathbb{R}^{257 \times 768}$  and  $\mathbf{f}^{VT} \in \mathbb{R}^{77 \times 768}$  from fMRI voxels, which are supervised by coarse- and fine-grained features,  $\mathbf{f}^T$  and  $\mathbf{f}^I$ , respectively. We adopt the Mean Squared Error loss for the accurate prediction of CLIP embeddings:

$$\mathcal{L}_H = \|\mathbf{f}^T - \mathbf{f}^{VT}\|_2^2 + \|\mathbf{f}^I - \mathbf{f}^{VI}\|_2^2. \quad (2)$$

By simultaneously decoding multi-granularity high-level semantics and low-level details, this pipeline achieves a balance between semantic fidelity and low-level attributes such as spatial structure and color composition. However, directly learning a mapping between fMRI and the semantic features is prone to overfitting [20], which is essentially caused by information asymmetry. To tackle this issue, we propose CIM and CCM to explore richer semantic patterns inspired by human visual cognition, thereby alleviating the modality gap.

#### B. Cognitive Integration Module

The information asymmetry between fMRI and images partly arises from the fact that humans perceive objects regionally, guided by holistic prior knowledge [26], whereas images are typically processed at the patch or global level.

To mitigate this issue, we propose the Cognitive Integration Module (CIM), which is shown in Fig. 4, to enhance regional fMRI representations and reduce information asymmetry. It simulates human prior knowledge via prototypes from annotated semantic masks, and complements finer-grained patterns from unsupervised clustering.

**Prototyping.** CIM aggregates regional representations under the prior guidance of the panoptic segmentation masks. We convert them into patch-level masks  $\mathbf{M} \in \mathbb{R}^{H \times W}$  ( $H$  and  $W$  denote patch token counts in height and width.) via majority voting, ensuring that each patch belongs to only one category. CIM derives the prototype  $p_m$  for semantic

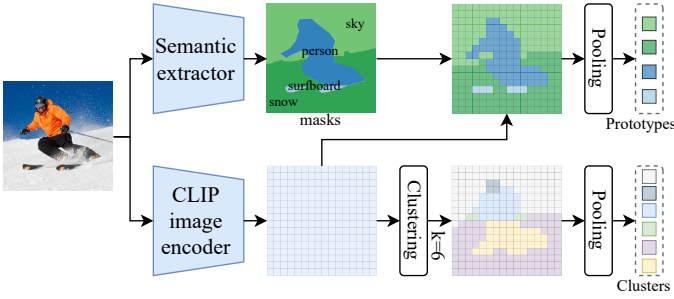


Fig. 4. Details of the CIM module. By employing panoptic segmentation masks and unsupervised clustering, we aggregate hierarchical regional semantics to simulate cognitive integration, improving intra-region semantic consistency.

category  $m$  from CLIP visual features  $f^{VI}$  via mask pooling, representing aggregated regional information:

$$\mathbf{p}_m = \frac{\sum \mathbf{f}_{i,j}^{VI} \cdot \mathbb{1}(\mathbf{M}_{i,j} = m)}{\sum \mathbb{1}(\mathbf{M}_{i,j} = m)}, m \in [0, C - 1], \quad (3)$$

where  $\mathbb{1}$  is an indicator denoting whether current patch belongs to category  $m$ ,  $C$  denotes the number of semantic categories.

**Clustering.** While semantic categories encode human prior knowledge, they overlook regional commonalities such as color and attributes. CIM complements them by adaptively aggregating regions through unsupervised clustering to capture finer-grained semantics. Specifically, CIM applies K-means [38] clustering to  $f^{VI}$  into  $K$  clusters, with the cluster center denoted as  $\mathbf{c}_k \in \mathbb{R}^{1 \times 768}$  for cluster  $k$ .

Both prototypes and clusters fundamentally capture multi-level visual region patterns. CIM employs MSE loss to incorporate them as additional supervision, enhancing semantic granularity for fMRI decoding. Furthermore, we introduce contrastive learning to guide fMRI features in distinguishing different region semantics, thereby enforcing intra-region semantic consistency. We denote the training process as  $\mathcal{L}_{CIM}$ :

$$\begin{aligned} \mathcal{L}_{CIM} = & \sum_{m=1}^C \frac{1}{N_c} \sum_{j \in \mathcal{C}_m} \left( \|\mathbf{f}_j^{VI} - \mathbf{p}_m\|_2^2 - \frac{\exp(\frac{\mathbf{f}_j^{VI} \cdot \mathbf{p}_m}{\tau})}{\sum_{i=1}^C \exp(\frac{\mathbf{f}_j^{VI} \cdot \mathbf{p}_i}{\tau})} \right) \\ & + \sum_{k=1}^K \frac{1}{N_k} \sum_{j \in \mathcal{C}_k} \left( \|\mathbf{f}_j^{VI} - \mathbf{c}_k\|_2^2 - \frac{\exp(\frac{\mathbf{f}_j^{VI} \cdot \mathbf{c}_k}{\tau})}{\sum_{i=1}^K \exp(\frac{\mathbf{f}_j^{VI} \cdot \mathbf{c}_i}{\tau})} \right), \end{aligned} \quad (4)$$

where  $\mathcal{C}_m$  and  $\mathcal{C}_k$  are the sets of tokens belonging to the corresponding prototype  $m$  and cluster  $k$ , respectively.  $N_c$  and  $N_k$  denote the number of their respective token sets.  $\tau$  is the temperature parameter in contrastive learning.

By integrating multi-level semantic aggregation with contrastive learning, CIM enhances semantic consistency within regions, leading to faithful reconstruction of object details.

### C. Cognitive Correlation Module

CIM introduces multi-level semantics to ensure intra-region consistency, yet it is also crucial to capture contextual relationships for fMRI decoding. To this end, we propose the Cognitive Correlation Module (CCM), enabling fMRI features to

learn the topological relationships among semantics motivated by the human differential perception process [27], [28].

Specifically, CCM learns fine- and coarse-grained semantic contextual relationships from CLIP visual and text features, respectively. The relationships are established via Cosine distance, denoted as  $\epsilon(\cdot)$ . The training objective of CCM is:

$$\mathcal{L}_{CCM} = \|\epsilon(\mathbf{f}^I) - \epsilon(\mathbf{f}^{VI})\|_1 + \|\epsilon(\mathbf{f}^T) - \epsilon(\mathbf{f}^{VT})\|_1, \quad (5)$$

where the fine-grained relationship matrix of  $\mathbf{f}^{VI}$  is  $\mathbb{R}^{257 \times 257}$  and coarse-grained relationship matrix of  $\mathbf{f}^{VT}$  is  $\mathbb{R}^{77 \times 77}$ .

The topological relationships of visual stimuli in the CLIP representation space serves as prior knowledge to guide fMRI decoding, mitigating the spatial layout inconsistencies and structural misplacement. CCM further facilitates the fidelity of inter-region relationships between elements in visual stimuli based on more complete elements or attributes from CIM.

### D. Training And Inference

During the training process, the above two modules simultaneously provide semantic guidance for fMRI decoding. In summary, the final training objective of BrainCognizer is:

$$\mathcal{L}_{total} = \mathcal{L}_L + \mathcal{L}_H + \mathcal{L}_{CIM} + \mathcal{L}_{CCM}. \quad (6)$$

During inference, only brain signals are needed and processed by the encoder to obtain the low-level feature  $\mathbf{f}^{VL}$  and high-level semantic features  $\mathbf{f}^{VT}$ ,  $\mathbf{f}^{VI}$ . The low-level feature is subsequently input to the VAE decoder, producing a low-level image with blurred color and contour information, which serves as the initialization for Versatile Diffusion. Finally, the semantic features serve as conditions to provide controllable guidance for image generation in the diffusion model.

## IV. EXPERIMENTS

### A. Experimental Settings

1) *Dataset:* We conduct experiments on the Natural Scenes Dataset (NSD) [39], the largest public fMRI dataset for image reconstruction. Following previous methods [16]–[19], [33], [40], we use fMRI data from four participants who viewed three repetitions of complex natural images from the MSCOCO dataset [41]. We adopt the official `nsdgeneral` region of interest (ROI) mask for the visual cortex, which spans early to high-order visual areas, consistent with prior works. The fMRI data within the selected ROI are flattened into a 1D voxel sequence for decoding. For each subject, the training set consists of 8,859 unique image stimuli and 24,980 fMRI trials (with up to three per image). The test set contains 982 shared images and 2,770 trials across all four subjects.

2) *Evaluation Metrics:* We evaluate low-level reconstruction quality using four metrics: Pixelwise Correlation (Pix-Corr), Structural Similarity Index (SSIM) [42], and two-way identification based on features from AlexNet’s second and fifth layers [43]. For high-level reconstruction evaluation, we adopt four additional metrics: two-way identification with Inception [44] and CLIP [12], as well as average correlation distance with EfficientNet-B1 [45] and SwAV-ResNet50 [46], following previous studies [16]–[19], [33], [40].

TABLE I

QUANTITATIVE COMPARISON OF RECONSTRUCTION PERFORMANCE WITH SOTA MODELS. SOME METHODS ARE EXCLUDED BECAUSE THEY ARE NOT OPEN-SOURCE OR USED ADDITIONAL DATA. ALL METRICS ARE AVERAGED OVER SUBJECTS 1, 2, 5, AND 7. THE BEST RESULTS ARE HIGHLIGHTED IN BOLD, AND THE SECOND-BEST RESULTS ARE UNDERLINED. ARROWS INDICATE THAT HIGHER OR LOWER VALUES ARE PREFERABLE.

Method	Low-Level				High-Level			
	PixCorr $\uparrow$	SSIM $\uparrow$	Alex(2) $\uparrow$	Alex(5) $\uparrow$	Incep $\uparrow$	CLIP $\uparrow$	EffNet-B $\downarrow$	SwAV $\downarrow$
Ozcelik et al. [32] (IJCNN 2022)	.126	.135	68.9%	81.2%	76.4%	76.3%	.879	.579
Mind-Reader [30] (NIPS 2022)	.104	.294	70.9%	83.9%	78.2%	78.1%	.853	.463
Takagi et al. [18] (CVPR 2023)	.222	.318	83.0%	83.0%	76.0%	77.0%	.916	.578
Gu et al. [33] (MIDL 2023)	.082	.297	68.9%	79.9%	75.2%	70.4%	.901	.501
Brain-Diffuser [16] (Sci. Rep 2023)	.254	<b>.356</b>	94.2%	96.2%	87.2%	91.5%	.775	.423
MindEye [17] (NeurIPS 2023)	<u>.309</u>	.323	<b>94.7%</b>	<b>97.8%</b>	<u>93.8%</u>	94.1%	<b>.645</b>	<u>.367</u>
MindDiffuser [25] (MM 2023)	.256	.344	85.2%	84.3%	78.4%	79.1%	.884	.551
MindBridge [19] (CVPR 2024)	.148	.259	86.9%	95.3%	92.2%	94.3%	<u>.713</u>	.413
DREAM [6] (WACV 2024)	.274	.328	93.9%	96.7%	93.4%	94.1%	<b>.645</b>	.410
<b>BrainCognizer</b>	<b>.319</b>	<u>.346</u>	<u>94.5%</u>	<u>97.5%</u>	<b>94.8%</b>	<b>95.3%</b>	<b>.645</b>	<b>.365</b>

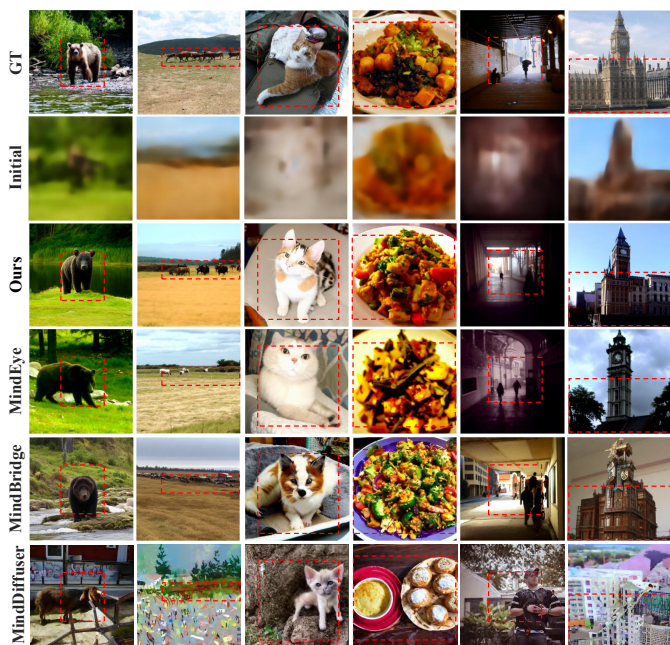


Fig. 5. Qualitative comparison of reconstruction examples on subject 1 given input fMRI signals. The highlighted regions indicate comparison. We reconstruct more fine-grained semantic attributes (e.g., the 1st and 6th columns), while also preserve more consistent spatial layout (e.g., the 5th column).

3) *Implementation Details*: The experiments are conducted using 2 NVIDIA RTX 4090 GPUs, with a batch size set to 50 per GPU. Our learning rate is set to  $3e-4$ ,  $\tau$  in Eq. 4 is  $5e-2$ , and we use the AdamW strategy to train for 200 epochs.

### B. Comparisons With SOTA Methods

1) *Quantitative Comparison*: We report the average performance of the model across four subjects in terms of both high-level semantic relevance and low-level pixel similarity. As shown in Tab. I, BrainCognizer exhibits robust performance, achieving state-of-the-art (SOTA) results on five evaluation metrics and ranking second on the remaining three. It exhibits

a significant advantage in high-level semantic evaluations, indicating that incorporating multi-level intra-region semantics and inter-region semantic correlations enables more comprehensive decoding of visual semantics from fMRI.

Notably, under the same CLIP and diffusion model settings as MindBridge, BrainCognizer achieves an average improvement of 6.4% across the eight evaluation metrics. Compared with MindEye, we do not introduce any additional network structures, yet still achieve even superior performance without incurring extra computational cost.

BrainCognizer simulates the human visual cognition to effectively extract meaningful semantics from fMRI signals and achieves the highest CLIP score, thereby providing a powerful learning paradigm for fMRI representation that bridges the modality gap through alignment with CLIP embeddings.

2) *Qualitative Comparison*: The reconstruction images in Fig. 2 and Fig. 5 demonstrate the effectiveness of BrainCognizer. BrainCognizer preserves intra-region semantic consistency and image details, such as the bear’s ears (1st column) and the building (6th column). It also better preserves inter-region semantic correlations reflected in consistent spatial and contextual layouts, such as the vegetable arrangement (4th column) and the lighting structure (5th column). Moreover, BrainCognizer uses fMRI-decoded images (2nd row) to initialize diffusion, reducing randomness and enhancing consistency.

### C. Robustness across subjects

Inter-subject variability in brain anatomy and neural responses leads to differences in fMRI signals, even under identical visual stimuli. To evaluate BrainCognizer’s generalizability, we reconstruct test images from subjects 1, 2, 5, and 7. As shown in Tab. III, despite the completely different training sets across the four subjects, we achieve comparable performance, especially on high-level metrics. The examples in Fig. 7 further support this finding, showing only minor stylistic differences across individuals, which indicates that our method generalizes well across subjects.

### D. Ablation Study

TABLE II  
ABLATION STUDY OF OUR COMPONENTS. THE BEST RESULT IS HIGHLIGHTED IN BOLD, AND THE SECOND-BEST IS UNDERLINED.

Modules	CIM CCM	$\times$ $\times$	$\checkmark$ $\times$	$\times$ $\checkmark$	$\checkmark$ $\checkmark$
Low-Level	PixCorr $\uparrow$	.394	.398	<u>.405</u>	<b>.406</b>
	SSIM $\uparrow$	.347	.351	<b>.367</b>	<u>.364</u>
	Alex(2) $\uparrow$	96.9%	<b>97.7%</b>	96.9%	<u>97.5%</u>
	Alex(5) $\uparrow$	98.1%	<u>98.5%</u>	97.8%	<b>98.6%</b>
High-Level	Incep $\uparrow$	92.8%	<u>94.9%</u>	93.8%	<b>95.3%</b>
	CLIP $\uparrow$	93.9%	<u>95.1%</u>	94.3%	<b>96.0%</b>
	EffNet-B $\downarrow$	.715	<u>.649</u>	.657	<b>.641</b>
	SwAV $\downarrow$	.407	<u>.371</u>	.379	<b>.360</b>

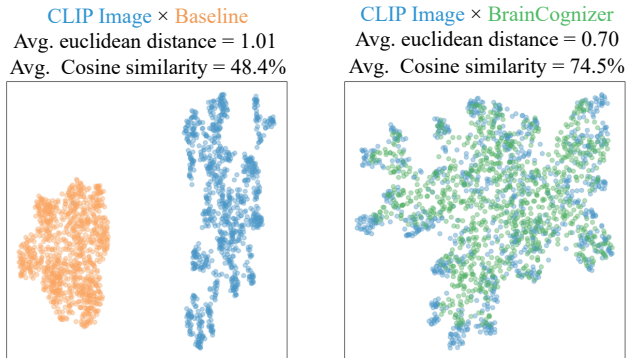


Fig. 6. UMAP [47] visualizations of the CLIP (blue), Baseline (orange), and our BrainCognizer (green). The UMAPs are estimated from 982 samples in the testing set.

We progressively incorporate each module into BrainCognizer to evaluate their individual contributions to the final performance on Subject 1, as shown in Tab. II. Our proposed pipeline serves as a strong baseline, demonstrating balanced performance across all eight evaluation metrics.

Since the human visual system is insensitive to low-level variations, high-level metrics are considered more indicative of perceptual reconstruction quality [48]. On high-level metrics, our method achieves an average improvement of 4.2%, with CIM and CCM individually contributing 3.4% and 2.5%, respectively, while maintaining performance on low-level metrics. The integration of the proposed modules enables more effective preservation of rich semantic information from visual stimuli and improves the alignment between fMRI representations and reconstructed images. Ablation studies demonstrate that incorporating additional semantic and relational information is crucial for accurately aligning reconstructed images with the original visual stimuli at a fine-grained level.

As shown in Fig. 6, our semantic constraints improve cross-modal alignment and better leverage CLIP’s semantic encoding. Furthermore, we calculate the Cosine similarity between fMRI-derived semantic features and image semantic features, achieving a 53.8% improvement over the baseline. The Euclidean distance also decreases by 30.4%, indicating that BrainCognizer successfully aligns the two embedding spaces and reduces the modality gap. Leveraging brain-

TABLE III  
RESULTS ON SUBJECTS 1, 2, 5, AND 7.

	Metric	Sub 1	Sub 2	Sub 5	Sub 7
Low-Level	PixCorr $\uparrow$	.406	.327	.277	.264
	SSIM $\uparrow$	.364	.348	.338	.335
	Alex(2) $\uparrow$	97.5%	95.7%	92.8%	92.0%
	Alex(5) $\uparrow$	98.6%	97.9%	97.4%	95.9%
High-Level	Incep $\uparrow$	95.3%	94.8%	95.6%	93.3%
	CLIP $\uparrow$	96.0%	94.6%	96.7%	93.9%
	EffNet-B $\downarrow$	.641	.650	.619	.669
	SwAV $\downarrow$	.360	.364	.353	.381

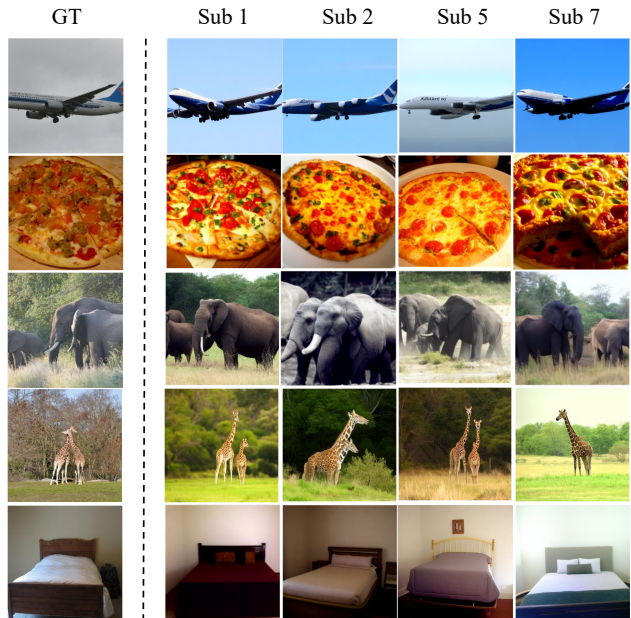


Fig. 7. Our reconstruction visualization on subjects 1, 2, 5, and 7. These results demonstrate that Braincognizer exhibits inter-subject consistency and generalization.

inspired perception, our method fuses fine-grained semantics, enhancing generalization and mitigating overfitting.

### E. Hyperparameter analysis

To investigate the sensitivity of cluster numbers in CIM, Tab. IV presents a comparative evaluation of BrainCognizer under different cluster numbers, which shows low sensitivity of  $k$  with stable low-level pixel and structural similarity. The K-means clustering provides finer-grained semantics compared to prototypes, enabling the integration of hierarchical semantic cues across different values of  $k$ . Cluster sizes of  $k = 15, 20,$  and  $25$  achieve a favorable trade-off between diversity and representational capacity. Based on this analysis,  $k = 15$  is adopted in the final model.

### F. Neuroscience interpretability

We investigate the interpretability of decoded features from a neuroscience perspective by mapping them onto brain voxel activations. We employ the L2-regularized linear regression to automatically select voxels for fitting decoded features, and

TABLE IV  
PERFORMANCE OF BRAINCognizer WITH DIFFERENT NUMBERS OF CLUSTERS  $k$  ON SUBJECT 1. BOLD VALUES HIGHLIGHT THE BEST RESULTS FOR EACH METRIC.

Metric	Baseline	BrainCognizer				
		k=5	k=10	k=15	k=20	k=25
PixCorr $\uparrow$	0.394	0.405	0.405	<b>0.406</b>	0.405	<b>0.406</b>
SSIM $\uparrow$	0.347	0.362	0.361	<b>0.364</b>	0.363	<b>0.364</b>
Alex(2) $\uparrow$	96.90%	97.6%	<b>97.7%</b>	97.5%	97.6%	97.5%
Alex(5) $\uparrow$	98.10%	<b>98.6%</b>	98.5%	<b>98.6%</b>	<b>98.6%</b>	98.5%
Incep $\uparrow$	92.80%	95.0%	94.9%	95.3%	95.1%	<b>95.5%</b>
CLIP $\uparrow$	93.90%	95.5%	95.6%	<b>96.0%</b>	95.9%	95.9%
EffNet-B $\downarrow$	0.715	0.644	0.641	0.641	<b>0.637</b>	<b>0.637</b>
SwAV $\downarrow$	0.407	0.362	0.361	0.360	<b>0.359</b>	0.360

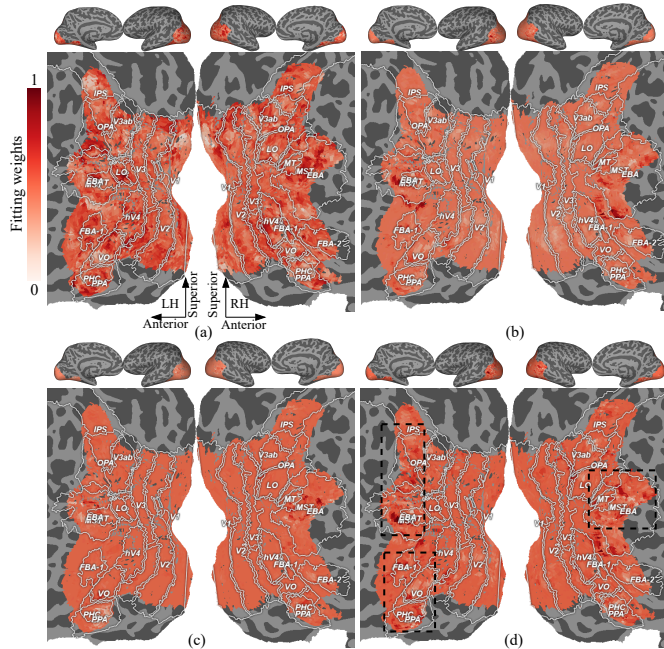


Fig. 8. ROI-wise importance in decoding information. Regression weights are mapped onto the 2D flat cortex map with ROI labels. Red indicates stronger decoding contributions. We visualize the activations of: (a) low-level features of VAE, (b) fine-grained semantic features from CLIP image encoder, (c) coarse-grained semantic features from CLIP text encoder, (d) hierarchical intra-region semantic features of CIM.

project the weights onto the 3D brain cortex. BrainCognizer decodes multi-level semantic information from fMRI and maps it to visual cortical areas to analyze activation-based patterns.

As shown in Fig. 8(a), low-level features activate most visual cortical areas, especially early regions (V1–V4) related to color and shape. In Fig. 5 (second row), low-level features provide initialization cues (e.g., color, layout) consistent with corresponding cortical functions. As shown in Fig. 8(b) and (c), decoding CLIP image and caption features yields relatively uniform activation across visual regions, with slight emphasis in higher-order areas like EBA, FBA-1, and FBA-2, suggesting their role in visual semantic processing. Although these features activate visual-related cortical regions, they have not fully captured the visual pattern embedded in voxels within higher-order brain areas. BrainCognizer effectively addresses

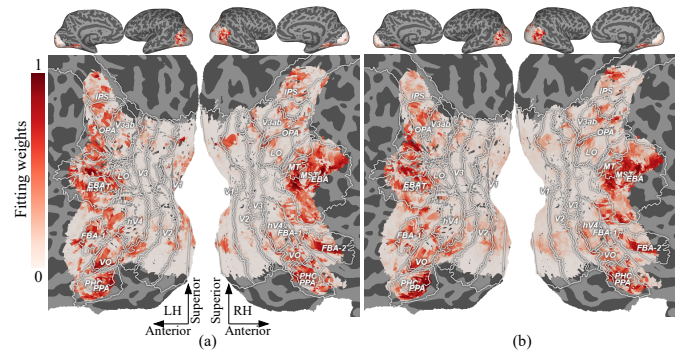


Fig. 9. ROI-wise importance in decoding. We visualize the activations of: (a) correlation of coarse-grained features in CCM, (b) correlation of fine-grained features in CCM.

this limitation. In Fig. 8(d), the intra-region semantic features from CIM elicit stronger activation in several high-order ROIs, including the EBA, OPA, PPA, and IPS, which are involved in advanced visual processing and semantic integration.

Besides, Fig. 9 (a) and (b) further illustrate the cortical activation corresponding to the semantic correlations from CCM. The results show widespread activation across high-order visual-related ROIs involved in object recognition, scene perception, and spatial-semantic integration, especially in the IPS, PPA, and OPA. This activation suggests that the decoding of semantic correlations relies on abstract and structured semantic representations in high-level visual areas, further supporting the neural plausibility of our method.

By integrating CIM and CCM, BrainCognizer effectively extracts more semantic patterns in high-order cortices compared with the original pipeline. It increases the information density of fMRI decoding and mitigates inter-modal asymmetry. These results provide physiological evidence supporting the effectiveness of the proposed CIM and CCM.

## V. CONCLUSION

To mitigate the information asymmetry between brain signals and visual stimuli, this paper proposes BrainCognizer, a novel brain decoding framework inspired by human visual cognition. BrainCognizer incorporates the Cognitive Integration Module and the Cognitive Correlation Module, to extract hierarchical region semantics guided by human prior knowledge and capture contextual semantic relationships across regions, respectively. They effectively enhances intra-region semantic consistency and preserves inter-region contextual relationships. Furthermore, we analyze the interpretability of the components from a neuroscientific perspective. Extensive experiments demonstrate that BrainCognizer achieves state-of-the-art performance across multiple evaluation metrics.

## ACKNOWLEDGMENTS

This work was supported by National Natural Science Foundation of China (grant No. 62376068, 62350710797, U24A20340), by Guangdong Basic and Applied Basic Research Foundation (grant No. 2023B1515120065), by Shen-

## REFERENCES

- [1] S. Ogawa, T.-M. Lee, A. S. Nayak, and P. Glynn, "Oxygenation-sensitive contrast in magnetic resonance image of rodent brain at high magnetic fields," *Magn Reson Med*, vol. 14, no. 1, pp. 68–78, 1990.
- [2] D. G. Cerdas, C. Sartzetaki, M. Petersen, G. Roig, P. Mettes, and I. Groen, "BrainACTIV: Identifying visuo-semantic properties driving cortical selectivity using diffusion-based image manipulation," in *ICLR*, 2025.
- [3] W. Guo, G. Sun, J. He, T. Shao, S. Wang, Z. Chen, M. Hong, Y. Sun, and H. Xiong, "A survey of fmri to image reconstruction," *arXiv:2502.16861*, 2025.
- [4] A. Luo, J. Yeung, R. Zawar, S. R. Dewan, M. M. Henderson, L. Wehbe, and M. J. Tarr, "Brain mapping with dense features: Grounding cortical semantic selectivity in natural images with vision transformers," in *ICLR*, 2025.
- [5] R. Belyi, G. Gaziv, A. Hoogi, F. Strappini, T. Golan, and M. Irani, "From voxels to pixels and back: Self-supervision in natural-image reconstruction from fmri," *NIPS*, vol. 32, pp. 6514–6524, 2019.
- [6] W. Xia, R. De Charette, C. Oztireli, and J.-H. Xue, "Dream: Visual decoding from reversing human visual system," in *WACV*, 2024, pp. 8226–8235.
- [7] P.-A. Comby, Z. Amor, A. Vignaud, and P. Ciuciu, "Denoising of fmri volumes using local low rank methods," in *ISBI*, 2023, pp. 1–5.
- [8] G. St-Yves and T. Naselaris, "Generative adversarial networks conditioned on brain activity reconstruct seen images," in *SMC*. IEEE, 2018, pp. 1054–1061.
- [9] K. Seeliger, U. Güçlü, L. Ambrogioni, Y. Güçlütürk, and M. A. Van Gerven, "Generative adversarial networks for reconstructing natural images from brain activity," *NeuroImage*, vol. 181, pp. 775–785, 2018.
- [10] Y. Lin, J. Li, and H. Wang, "Dcnn-gan: Reconstructing realistic image from fmri," in *MVA*. IEEE, 2019, pp. 1–6.
- [11] Z. Ren, J. Li, X. Xue, X. Li, F. Yang, Z. Jiao, and X. Gao, "Reconstructing seen image from brain activity by visually-guided cognitive representation and adversarial learning," *NeuroImage*, vol. 228, p. 117602, 2021.
- [12] A. Radford, J. W. Kim, C. Hallacy, A. Ramesh, G. Goh, S. Agarwal, G. Sastry, A. Askell, P. Mishkin, J. Clark *et al.*, "Learning transferable visual models from natural language supervision," in *ICML*, 2021, pp. 8748–8763.
- [13] J. Ho, A. Jain, and P. Abbeel, "Denoising diffusion probabilistic models," *NIPS*, vol. 33, pp. 6840–6851, 2020.
- [14] R. Rombach, A. Blattmann, D. Lorenz, P. Esser, and B. Ommer, "High-resolution image synthesis with latent diffusion models," in *CVPR*, 2022, pp. 10 684–10 695.
- [15] X. Xu, Z. Wang, G. Zhang, K. Wang, and H. Shi, "Versatile diffusion: Text, images and variations all in one diffusion model," in *ICCV*, 2023, pp. 7754–7765.
- [16] F. Ozcelik and R. VanRullen, "Natural scene reconstruction from fmri signals using generative latent diffusion," *Sci. Rep.*, vol. 13, no. 1, p. 15666, 2023.
- [17] P. Scotti, A. Banerjee, J. Goode, S. Shabalin, A. Nguyen, A. Dempster, N. Verlinde, E. Yundler, D. Weisberg, K. Norman *et al.*, "Reconstructing the mind's eye: fmri-to-image with contrastive learning and diffusion priors," *NIPS*, vol. 36, 2024.
- [18] Y. Takagi and S. Nishimoto, "High-resolution image reconstruction with latent diffusion models from human brain activity," in *CVPR*, 2023, pp. 14 453–14 463.
- [19] S. Wang, S. Liu, Z. Tan, and X. Wang, "Mindbridge: A cross-subject brain decoding framework," in *CVPR*, 2024, pp. 11 333–11 342.
- [20] Y. Lu, C. Du, C. Wang, X. Zhu, L. Jiang, X. Li, and H. He, "Animate your thoughts: Reconstruction of dynamic natural vision from human brain activity," in *ICLR*, 2025.
- [21] D. J. Felleman and D. C. Van Essen, "Distributed hierarchical processing in the primate cerebral cortex." *Cerebral cortex (New York, NY: 1991)*, vol. 1, no. 1, pp. 1–47, 1991.
- [22] K. Grill-Spector and K. S. Weiner, "The functional architecture of the ventral temporal cortex and its role in categorization," *Nat. Rev. Neurosci.*, vol. 15, no. 8, pp. 536–548, 2014.
- [23] D. J. Kravitz, K. S. Saleem, C. I. Baker, and M. Mishkin, "A new neural framework for visuospatial processing," *Nat. Rev. Neurosci.*, vol. 12, no. 4, pp. 217–230, 2011.
- [24] A. G. Huth, S. Nishimoto, A. T. Vu, and J. L. Gallant, "A continuous semantic space describes the representation of thousands of object and action categories across the human brain," *Neuron*, vol. 76, no. 6, pp. 1210–1224, 2012.
- [25] Y. Lu, C. Du, Q. Zhou, D. Wang, and H. He, "Minddiffuser: Controlled image reconstruction from human brain activity with semantic and structural diffusion," in *ACM MM*, 2023, pp. 5899–5908.
- [26] K. Koffka, "Perception: an introduction to the gestalt-theorie." *Psychol. Bull.*, vol. 19, no. 10, p. 531, 1922.
- [27] R. H. Masland, "The neuronal organization of the retina," *Neuron*, vol. 76, no. 2, pp. 266–280, 2012.
- [28] T. Poggio and S. Edelman, "A network that learns to recognize three-dimensional objects," *Nature*, vol. 343, no. 6255, pp. 263–266, 1990.
- [29] Y. Liu, Y. Ma, W. Zhou, G. Zhu, and N. Zheng, "Brainclip: Bridging brain and visual-linguistic representation via clip for generic natural visual stimulus decoding," *arXiv:2302.12971*, 2023.
- [30] S. Lin, T. Sprague, and A. K. Singh, "Mind reader: Reconstructing complex images from brain activities," *NIPS*, vol. 35, pp. 29 624–29 636, 2022.
- [31] T. Fang, Y. Qi, and G. Pan, "Reconstructing perceptive images from brain activity by shape-semantic gan," *NIPS*, vol. 33, pp. 13 038–13 048, 2020.
- [32] F. Ozcelik, B. Choksi, M. Mozafari, L. Reddy, and R. VanRullen, "Reconstruction of perceived images from fmri patterns and semantic brain exploration using instance-conditioned gans," in *IJCNN*. IEEE, 2022, pp. 1–8.
- [33] Z. Gu, K. Jamison, A. Kuceyeski, and M. R. Sabuncu, "Decoding natural image stimuli from fMRI data with a surface-based convolutional network," in *MIDL*, 2024, pp. 107–118.
- [34] H. Yang, J. Gee, and J. Shi, "Brain decodes deep nets," in *CVPR*, 2024, pp. 23 030–23 040.
- [35] A. Y. Wang, K. Kay, T. Naselaris, M. J. Tarr, and L. Wehbe, "Better models of human high-level visual cortex emerge from natural language supervision with a large and diverse dataset," *Nat. Mach. Intell.*, vol. 5, no. 12, pp. 1415–1426, 2023.
- [36] Q. Zhou, C. Du, S. Wang, and H. He, "Clip-mused: Clip-guided multi-subject neural information neuroscience and artificial intelligence," in *ICLR*, 2024.
- [37] D. P. Kingma and M. Welling, "Auto-encoding variational bayes," *arXiv preprint arXiv:1312.6114*, 2013.
- [38] J. MacQueen, "Some methods for classification and analysis of multivariate observations," in *Berkeley Symp. on Math. Statist. and Prob.*, vol. 5, 1967, pp. 281–298.
- [39] E. J. Allen, G. St-Yves, Y. Wu, J. L. Breedlove, J. S. Prince, L. T. Dowdle, M. Nau, B. Caron, F. Pestilli, I. Charest *et al.*, "A massive 7t fmri dataset to bridge cognitive neuroscience and artificial intelligence," *Nat. Neurosci.*, vol. 25, no. 1, pp. 116–126, 2022.
- [40] I. Han, J. Lee, and J. C. Ye, "Mindformer: A transformer architecture for multi-subject brain decoding via fmri," *arXiv:2405.17720*, 2024.
- [41] T.-Y. Lin, M. Maire, S. Belongie, J. Hays, P. Perona, D. Ramanan, P. Dollár, and C. L. Zitnick, "Microsoft coco: Common objects in context," in *ECCV*, 2014, pp. 740–755.
- [42] Z. Wang, A. C. Bovik, H. R. Sheikh, and E. P. Simoncelli, "Image quality assessment: from error visibility to structural similarity," *TIP*, vol. 13, no. 4, pp. 600–612, 2004.
- [43] A. Krizhevsky, I. Sutskever, and G. E. Hinton, "Imagenet classification with deep convolutional neural networks," *NIPS*, vol. 25, pp. 1106–1114, 2012.
- [44] C. Szegedy, V. Vanhoucke, S. Ioffe, J. Shlens, and Z. Wojna, "Rethinking the inception architecture for computer vision," in *CVPR*, 2016, pp. 2818–2826.
- [45] M. Tan and Q. Le, "Efficientnet: Rethinking model scaling for convolutional neural networks," in *ICML*, 2019, pp. 6105–6114.
- [46] M. Caron, I. Misra, J. Mairal, P. Goyal, P. Bojanowski, and A. Joulin, "Unsupervised learning of visual features by contrasting cluster assignments," *NIPS*, vol. 33, pp. 9912–9924, 2020.
- [47] L. McInnes, J. Healy, and J. Melville, "Umap: Uniform manifold approximation and projection for dimension reduction," *arXiv:1802.03426*, 2018.
- [48] J. Huo, Y. Wang, Y. Wang, X. Qian, C. Li, Y. Fu, and J. Feng, "Neuropictor: Refining fmri-to-image reconstruction via multi-individual pretraining and multi-level modulation," in *ECCV*, 2024, pp. 56–73.